Dynamic transitions of the magnetized spherical Couette flow between its base state and the return flow instability

Dynamic transitions of the magnetized spherical Couette flow between its base state and the return flow instability

J Ogbonna[1], F Garcia[2], T Gundrum[1], M Seilmayer[3] and F Stefani[1]

[1] Institute of Fluid Dynamics, Helmholtz-Zentrum Dresden-Rossendorf, Bautzner Landstr. 400, 01328 Dresden, Germany
[2] Universitat Politecnica de Catalunya, Escola d'Enginyeria de Barcelona Est, EEBE, Av. d'Eduard Maristany, 16, 08019 Barcelona, Spain
[3] SICK Engineering GmbH, Bergener Ring 27, 01458 Ottendorf-Okrilla, Germany

E-mail: j.ogbonna@hzdr.de

Abstract. The transition between the stable base state of the magnetized spherical Couette (MSC) flow and the return flow instability is experimentally investigated. The experiments are conducted using an MSC setup consisting of insulating spheres with the ratio of the inner to the outer radii $r_i/r_o = 0.5$, Reynolds number Re = 1000 and Hartmann number Ha $\in$ [25, 29]. The transition is characterized by changes in the power spectra of the azimuthal modes in the flow as Ha is dynamically changed. The transition occurs in the interval Ha $\in$ [26.5, 27.5]. The evolution of the power spectra of the azimuthal modes exhibits hysteretic effect depending on whether Ha is increased or decreased within the experimental interval. The power spectra in the azimuthal modes $m \in \{3, 4\}$ increases and remains dominant as Ha is increased, while the power spectra in $m \in \{2, 4\}$ are dominant while the flow is time dependent due to return flow instability as Ha is decreased.

1. Introduction

Spherical Couette flows are induced in fluids contained between two concentric spheres when the rotations of either one or both of the spheres cause the fluids to rotate differentially. If the fluid is electrically conducting and a magnetic field is applied, the resulting flow is referred to as a magnetized spherical Couette (MSC) flow. MSC flows are prevalent in astrophysical processes where ubiquitous amounts of plasmas and molten metals undergo differential rotation such as in the cores of the Sun, the planets and their moons.

MSC setups have been constructed as experimental devices to replicate various astrophysical processes in the laboratory to aid in their understanding. Experimental MSC setups are distinguished by the types of working fluids, the ratios of the radii of the inner to the outer spheres r_i/r_o, the electrical conductivities of the spheres and the configurations of the applied magnetic field. Liquid sodium with an electrically conducting inner sphere and an electrically insulating outer sphere has been used for MSC experiments with an axial magnetic field and $r_i/r_o = 0.33$ [1], and also with a dipolar magnetic field and $r_i/r_o = 0.35$ [2, 3, 4, 5]. The experiments in the present work are conducted with the HEDGEHOG (Hydromagnetic Experiment with Differentially Gyrating sphEres HOlding GaInSn) setup at Helmholtz-Zentrum Dresden-Rossendorf. HEDGEHOG uses GaInSn, a eutectic alloy of gallium (67% by mass), indium (20.5% by mass) and tin (12.5% by mass) as the working fluid. The ratio of the inner to the outer spheres $r_i/r_o = 0.5$, both spheres are electrically insulating, and an axial magnetic field is employed. Detailed descriptions of the experimental apparatus and the associated instrumentation are described in Section 3.

The simplest form of the MSC flow is where the inner sphere rotates while the outer sphere remains stationary. Such a flow is fully defined by four parameters, namely, the ratio of the radii of the inner to the outer spheres r_i/r_o, the Reynolds number $\mathrm{Re} = \Omega r_i^2/\nu$ (where Ω and ν are the rotation speed of the inner sphere and the kinematic viscosity of the fluid, respectively), the magnetic Prandtl number $\mathrm{Pm} = \nu/\eta$ (where η is the magnetic diffusivity of the fluid) and the Hartmann number $\mathrm{Ha} = B_0 r_i/(\mu_0 \rho \nu \eta)^2 = B_0 r_i \sigma^{1/2}/(\rho\nu)^{1/2}$ (where B_0, μ_0, ρ and σ are the applied magnetic field, vacuum permeability, the density of the fluid and the electrical conductivity of the fluid, respectively). Four different states of the MSC flow are generally identified, one of which is steady and the other three are time dependent. The steady state of the MSC is its base state, which consists of a flow driven by the rotation of the inner sphere. This rotation flings the fluid outwards by inertia, thus creating a secondary meridional circulation consisting of a narrow jet along the equator towards the outer sphere, and a return flow from the rest of the outer sphere towards the origin of the jet [6].

The time-dependent states of the MSC flow are commonly referred to as the radial jet, the return flow and the shear layer instabilities. The stability curves demarcating the parameter space of Re and Ha into regions representing the base state and the primary time-dependent (periodic) states of the MSC flow have been numerically computed for $r_i/r_o = 0.33$ [6], 0.5 [7] and 0.6 [7]. Each curve represents the azimuthal mode of the flow as the curve is crossed from the base state to the periodic state. The use of bifurcation lines representing a particular property of the flow is also used to graphically represent the MSC flow states. Since the base state is purely axisymmetric, it is convenient to represent the kinetic energy of the non-axisymmetric azimuthal modes $m \neq 0$ with the bifurcation lines [8] to demarcate the base state from the periodic states. The radial jet instability is triggered by the rotation of the inner sphere, when the magnetic field is absent or low, as Re exceeds its critical value. As a result, the jet adopts a wavy structure, alternatively slightly above and below the equatorial plane [6]. The return flow instability arises in the presence of a moderate magnetic field, and the instability is characterized by the concentration of the kinetic energy in the return flow of the meridional circulation. A further increase in the magnetic field results in the shear layer instability, where the kinetic energy is concentrated in the shear layers formed along the surface axially projected by the inner sphere as a result of the increased magnetic field.

HEDGEHOG has been used to conduct experiments to investigate the transitions of the MSC flow between its base and time-dependent states [9], and more recently to investigate the return flow instability [10]. The former experiments were conducted at fixed values of Ha, while the latter experiments were conducted with dynamically changing values of Ha (but entirely within the confines of the parameter space for the return flow instability). The aim of the present work is to combine the essence of the previous experiments by investigating the transition between the base state and the return flow instability with dynamically changing values of Ha. In doing so, the range of Ha where its critical value for the transition occurs can be estimated. Furthermore, by increasing and decreasing the Ha within the transition range, the hysteresis effect of the multistability of the azimuthal modes may be observed just as during the previous investigation of the return flow instability [10]. Hence, we expect the present work will supplement the previous one [10] by investigating the onset of the return flow instability.

2. Equations

If the spheres in the MSC flow rotate about $\hat{\mathbf{e}}_z$, the unit vector representing the z-axis, the axial magnetic field applied externally to the flow is given by B_0

$$\mathbf{B}_0 = B_0\hat{\mathbf{e}}_z = B_0 \cos(\theta)\,\hat{\mathbf{e}}_r - B_0 \sin(\theta)\,\hat{\mathbf{e}}_\theta \tag{1}$$

where B_0, θ, $\hat{\mathbf{e}}_r$ and $\hat{\mathbf{e}}_\theta$ are the magnetic field, the colatitude and the unit vectors representing the radial distance and the colatitude, respectively. The fluid flow $\mathbf{v}$ is governed by the Navier-Stokes equation

$$\partial_t \mathbf{v} + \mathbf{v}\cdot\nabla\mathbf{v} = -\nabla p + \mathrm{Re}^{-1}\nabla^2\mathbf{v} + \mathrm{Ha}^2\mathrm{Re}^{-1}(\nabla\times\mathbf{b})\times\hat{\mathbf{e}}_z \tag{2}$$

with the no-slip condition imposed at the boundaries between the fluid and both spheres. **b** is the deviation of the magnetic field induced by the interaction of the fluid flow with $\mathbf{B}_0$. For Rm << 1, this induced magnetic field is negligible compared to $\mathbf{B}_0$. This so-called inductionless approximation applies here, since all experiments were conducted at Re = 1000 and the Pm of GaInSn is in the order of 10^{-6}, resulting in Rm in the order of 10^{-3}. The induction equation simplifies then to

$$0 = \nabla^2\mathbf{b} + \nabla \times (\mathbf{v} \times \hat{\mathbf{e}}_z). \quad (3)$$

Insulating boundary conditions were considered in accordance with the experiments.

3. Experimental methods

3.1. Apparatus

The components of the HEDGEHOG setup are depicted in figure 1 (left). The acrylic glass inner and outer spheres have radii of 45 mm and 90 mm, respectively. The inner sphere is rotated by means of an electric motor shaft passing through the poles of both spheres. The diameter of the shaft inside the spheres is just 3 mm, so the interference which is very small relative to the interference on the overall flow of the fluid due to the rotation of the shaft is assumed to be insignificant. To act against the buoyancy force exerted by the relatively high density of GaInSn on the inner sphere, which is fully submerged in the fluid, a lead weight is contained within the inner sphere. The outer surface of the outer sphere contains provisions for mounting the ultrasonic transducers used for measuring the velocity of GaInSn. In addition, the surface contains 168 needle-like copper electrodes, providing the HEDGEHOG setup with the distinctive appearance that inspired its name. The copper electrodes enable the measurement of electric potential along the surface of the outer sphere if needed. The axial magnetic field for the flow is generated by a Helmholtz coil pair consisting of 80 wire windings in each coil. The distance between the coils and the radius of each coil are each approximately 300 mm.

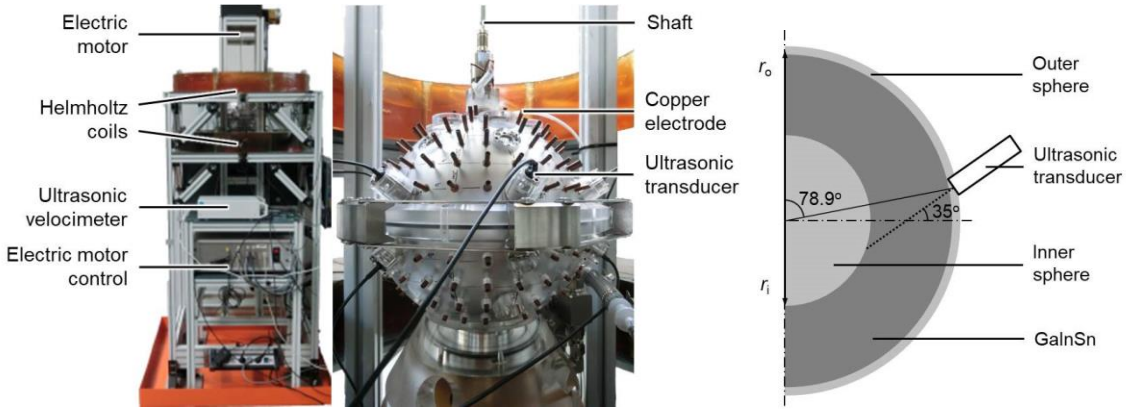

Figure 1. Left: photographs of the HEDGEHOG setup showing its full view and a close-up view on the outer sphere. Right: meridional section showing the geometric relations for one of the six azimuthally equidistant ultrasonic transducers installed on HEDGEHOG. The dotted line extending from the ultrasonic transducer represents its line of view along which the flow velocity components parallel to the line were measured.

3.2. Instrumentation

The ultrasonic Doppler velocimetry for measuring the velocity of GaInSn consists of piezoelectric ultrasonic transducers (Signal Processing SA, model TR0410LS) and an ultrasonic Doppler velocimeter (Signal Processing SA, model DOP3010). For the present experiments, six transducers were used at a colatitude of 78.9° with respect to the spheres. Each transducer was inclined southward so that the angle between the axis of the transducer and the equator of the spheres was 35°. Figure 1 (right) shows the geometric relationship between a transducer and the spheres. Each transducer

periodically emits an ultrasonic pulse at a frequency of 4 MHz and received the echoes from the particles in the path of the ultrasonic beam. These particles are formed as a result of the oxidation of GaInSn due to its exposure to air [11]. From each transducer channel, the velocimeter sequentially acquires the echo signals reflected by the particles to determine the velocities of the flow parallel to each transducer axis.

4. Results

Since ultrasonic Doppler velocimetry relies on the reflection of the ultrasonic pulses by the naturally-occurring oxides in GaInSn, the oxides were distributed by circulating the GaInSn from the north pole to the south pole via a peristaltic pump connected to the poles externally. The values of Re and Ha for the experiments were set using the properties of GaInSn listed in table 1. All experiments were conducted at Re = 1000. The magnetic field B_0 for the required Ha was set by the current I through the Helmholtz coil according to the relation

$$B_0 = (4/5)^{3/2}\, \mu_0 nI/R \tag{4}$$

where n is the number of wire windings in each Helmholtz coil and R is the radius of each coil and the distance between the coils.

Table 1. Physical properties of GaInSn from [12].

ρ (kg m^{-3})	ν (m^2 s^{-1})	$\eta = 1/\mu_0\sigma$ (m^2 s^{-1})
6.4×10^3	3.4×10^{-7}	0.2428

We first established the range of Ha within which the experiments were conducted. From numerical computations, for $r_i/r_o = 0.5$ and Re = 1000, the critical value of Ha at which the MSC flow transitions between the base state and the return flow instability is 25.8 [7]. Below this critical value, the MSC flow is in its base state but above the critical value, the flow becomes time dependent due to return flow instability. Previous experiments with HEDGEHOG showed that at Re = 1000 and Ha = 25, the flow was in its base state. Hence, the critical value of Ha for the flow in HEDGEHOG is at least 25, and this value was selected as the lower Ha bound for the experiments. Results from [10] showed that at Re = 1000, the flow was time dependent due to return flow instability at Ha = 27.5. This indicates that the critical value is below Ha = 27.5. However, in order to minimize the effect of uncertainties in the values Ha, the experimental range was widened by selecting Ha = 29 as the upper bound for the experiments. Therefore, the experiments were conducted at Ha $\in$ [25, 29] and the values of Ha were increased and decreased (linearly with time) between the limits. Each experiment was conducted for a period of 6 hours. In the subsequent sections, we first discuss the velocity profile of the flow during the experiments, and afterwards, the evolution of the azimuthal modes in the flow.

4.1. Velocities

Figure 2 and figure 3 show the plots of the velocity components of the flow along the axis of one of the six ultrasonic transducers as Ha was respectively increased and decreased between 25 and 29 (see top horizontal axes). The depths indicate the distance away from the transducer along its axis. The sign convention of the velocity is such that flows away from the transducers have positive velocities, while flows towards the transducers have negative velocities. Looking at figure 2, we see that the closer to the transducer, the flow has velocities that are nearly zero in value, while the flow velocities are negative further away from the transducer. The near-zero velocities close to the transducer are those of the return flow of the meridional circulation of the fluid. Since this flow is along the surface of the outer sphere, it cuts across the transducer axes nearly perpendicularly, thus registering velocities that are nearly zero. The negative velocities further away from the transducer are those of the radial jet of the meridional circulation. Since the radial jet originates from the inner sphere and flows towards the

outer sphere, and hence the transducers, it registers as having negative velocities. As Ha increases from 25 to 29, the influence of the return flow in the meridional circulation increases while diminishing the influence of the radial jet.

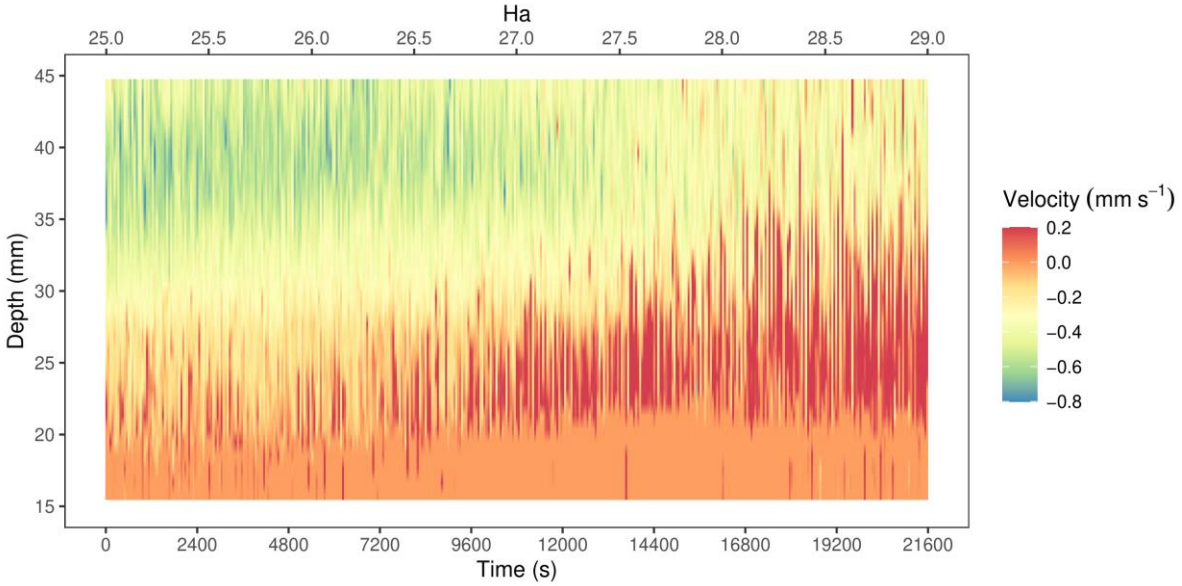

Figure 2. Plots of the experimentally measured velocity components parallel to the ultrasonic transducer axis as Ha was increased from 25 to 29. The depth indicates the axial distance from the ultrasonic transducer. Re = 1000.

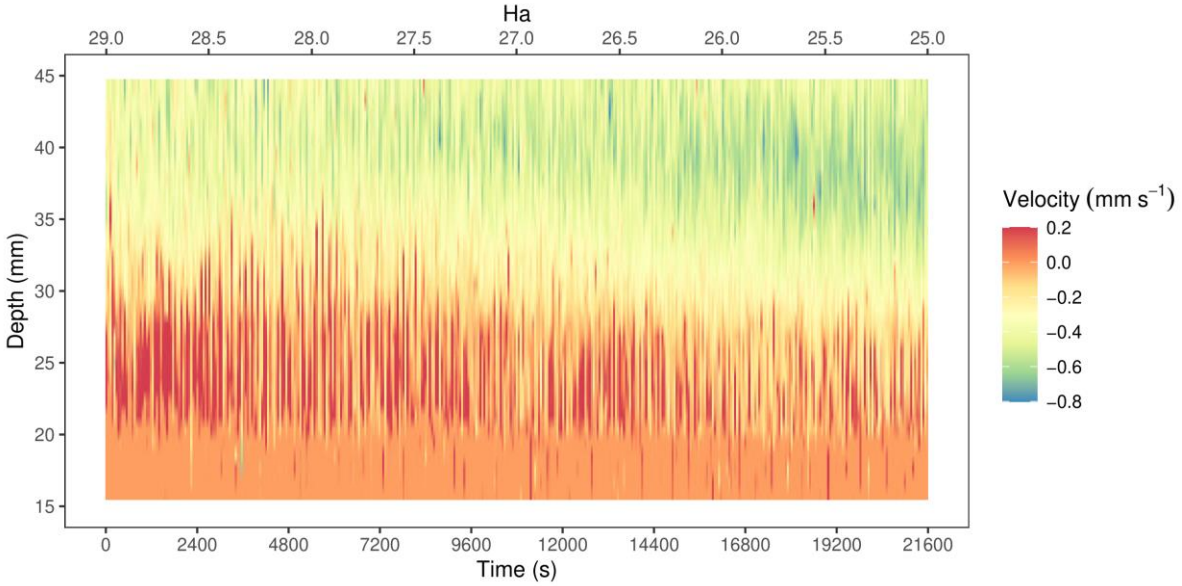

Figure 3. Plots of the experimentally measured velocity components parallel to the ultrasonic transducer axis as Ha was decreased from 25 to 29. The depth indicates the axial distance from the ultrasonic transducer. Re = 1000.

Since figure 2 and figure 3 were conducted within the same limits albeit from opposite ends, it is not surprising that the two plots resemble mirror images of each other. Consequently, earlier analyses of figure 2 applies to figure 3.

4.2. Azimuthal modes

It was mentioned in Section 1 that the base and time dependent states of the MSC flow differ by the absence of kinetic energy in the non-axisymmetric azimuthal modes in the former. Since the kinetic energy correlates with the power spectra of the azimuthal modes obtained from the Direct Fourier Transform (DFT) of the velocity-time data of the flow, the critical value of Ha for the flow transition in the experiments were estimated by the change in the power spectra of the azimuthal modes. The velocity-time data were divided into rectangular windows of 1080 seconds or Ha intervals of 0.2. Within each window, a two-dimensional DFT of the data in time and space (given by the positions of the six ultrasonic transducers) was conducted at a distance of 30 mm from the transducers, corresponding to coordinates of (r, θ) = (64 mm, 90°). The resulting amplitudes from the DFT were first squared, and then divided by twice the variance of the velocities in each window to obtain the normalized power spectra. The points in figure 4 and figure 5 indicate the root sum squares of the normalized power spectra in each azimuthal mode as Ha was respectively increased and decreased between 25 and 29. The curves indicate the locally estimated scatterplot smoothing (LOESS) of the points with a polynomial degree of 2 and a span of 0.5.

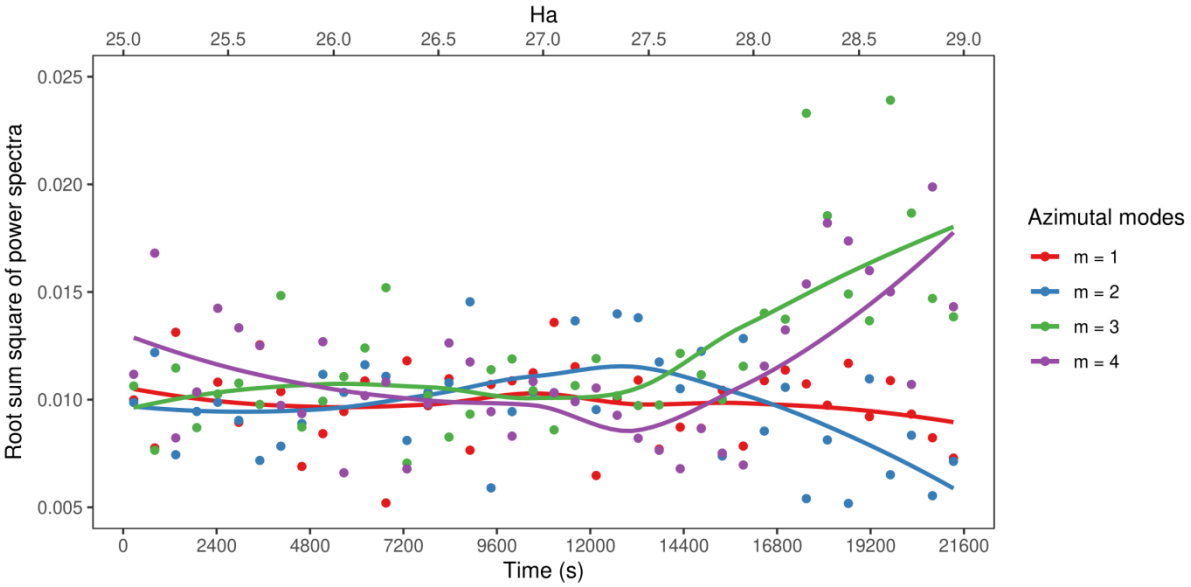

Figure 4. Root sum squares of the normalized power spectra in each azimuthal mode obtained from the DFT of the velocity-time data as Ha was increased from 25 to 29. Re = 1000.

Figure 4 shows that the power spectra of the azimuthal modes $m \in \{3, 4\}$ begin to increase within Ha $\in$ [27.0, 27.5]. Meanwhile, figure 5 shows that the power spectra in $m \in \{2, 4\}$ initially increase, as the flow increasingly becomes saturated, and then begins to decrease from Ha =27.5 until they fall to values similar to the rest of the azimuthal modes at around Ha = 27.5. Hence, the critical point of transition between the base state and the return flow instability for the experiments is in the interval Ha $\in$ [26.5, 27.5]. Given that the numerically computed critical value is Ha = 25.8, the discrepancy from the experimental result is approximately 3% to 7%.

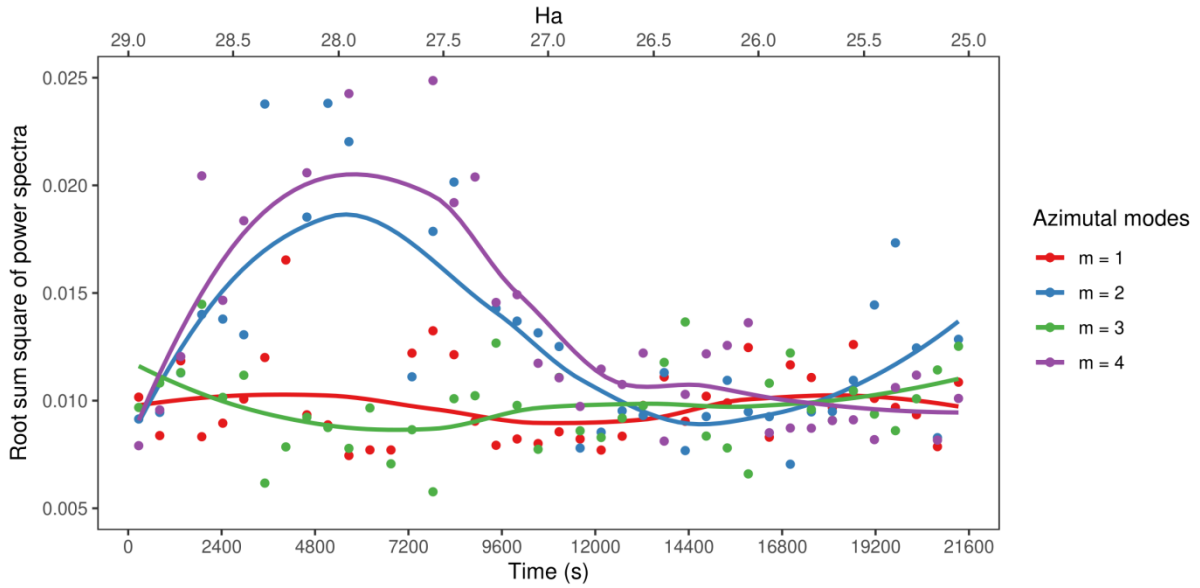

Figure 5. Root sum squares of the normalized power spectra in each azimuthal mode obtained from the DFT of the velocity-time data as Ha was decreased from 25 to 29. Re = 1000.

5. Conclusion

Experiments were conducted as the values of Ha were dynamically increased and decreased within the interval [25, 29] at Re = 1000, spanning the base state and the time dependent state due to return flow instability of the MSC flow. This was done in order to estimate the critical value of Ha for the transition and to observe the behavior of the system. The transition was characterized by the change in the power spectra (and hence, the kinetic energy) of the azimuthal modes in the MSC flow and was observed to occur within Ha ∈ [26.5, 27.5]. The evolution of the power spectra of the azimuthal modes exhibited hysteretic effects, as the power spectra in the azimuthal modes $m \in \{3, 4\}$ increased and remained dominant as Ha increased within the experimental interval, while power spectra in $m \in \{2, 4\}$ were dominant while the flow was time dependent due to return flow instability.

The azimuthal modes of the MSC flow correspond to the azimuthal symmetry of the waves in the flow. The simplest form of these waves are called rotating waves, which have been investigated for the return flow instability in [10]. A wave with one frequency – that of modulation – in addition to its frequency of rotation is referred to as a modulated rotating wave. Waves with two and even three additional frequencies have also been numerically computed [13]. Solutions to modulated rotating waves have been found through numerical simulations in the return flow instability, but since the range of Ha in which they the return flow instability is extremely narrow [14], detecting them experimentally is a challenging exercise. Fortunately, the range of Ha for the occurrence of modulated rotating waves in the radial jet instability is much wider [15] and it is very likely that they can be detected experimentally. Consequently, it is worthwhile to experimentally investigate the radial jet instability in detail.

6. References

[1] Sisan D R, Mujica N, Tillotson W A, Huang Y M, Dorland W, Hassam A B, Antonsen T M and Lathrop D P 2004 *Phys. Rev. Lett.* **93** 114502
[2] Schmitt D, Alboussière T, Brito D, Cardin P, Gagnière N, Jault D and Nataf H C 2008 *J. Fluid Mech.* **604** 175–197
[3] Nataf H C, Alboussiere T, Brito D, Cardin P, Gagnière N, Jault D and Schmitt D 2008 *Phys. Earth Planet. Inter.* **170** 60–72
[4] Brito D, Alboussière T, Cardin P, Gagnière N, Jault D, La Rizza P, Masson J P, Nataf H C and Schmitt D 2011 *Phys. Rev. E* **83** 066310
[5] Figueroa A, Schaeffer N, Nataf H C and Schmitt D 2013 *J. Fluid Mech.* **716** 445–469

[6] Hollerbach R 2009 *Proc. R. Soc. A* **465** 2003–2013
[7] Travnikov V, Eckert K and Odenbach S 2011 *Acta Mech.* **219** 255–268
[8] Garcia F and Stefani F 2018 *Proc. R. Soc. A* **474** 20180281
[9] Kasprzyk C, Kaplan E, Seilmayer M and Stefani F 2017 *Magnetohydrodynamics* **53** 393–401
[10] Ogbonna J, Garcia F, Gundrum T, Seilmayer M and Stefani F 2020 *Phys. Fluids* **32** 124119
[11] Borin D, Nikrityuk P and Odenbach S 2009 *Appl. Rheol.* **19** 61995
[12] Rüdiger G, Kitchatinov L L and Hollerbach R 2013 *Magnetic processes in astrophysics: theory, simulations, experiments* ISBN 978-3-527-41034-7
[13] Garcia F, Seilmayer M, Giesecke A and Stefani F 2020 *Chaos* **30** 043116
[14] Garcia F, Seilmayer M, Giesecke A and Stefani F 2019 *J. Nonlinear Sci.* **29** 2735–2759
[15] Garcia F, Seilmayer M, Giesecke A and Stefani F 2020 *Phys. Rev. Lett.* **125** 264501

Acknowledgments
This project has received funding from the European Research Council (ERC) under the European Union's Horizon 2020 research and innovation programme (Grant Agreement No. 787544).